Base–controlled Heck, Suzuki and Sonogashira reactions catalyzed by ligand–free platinum or palladium single-atom and sub–nanometer clusters

Estefanía Fernández, [†◊] Miguel A. Rivero–Crespo,[†◊] Irene Domínguez, [‡] Paula Rubio–Marqués, [†] Judit Oliver–Meseguer, [†] Lichen Liu, [†] María Cabrero–Antonino,[†] Rafael Gavara, [‡] Juan C. Hernández-Garrido, [§] Mercedes Boronat, *,[†] Antonio Leyva–Pérez,*, [†] and Avelino Corma. *,[†]

[†] Instituto de Tecnología Química (UPV–CSIC), Universitat Politècnica de València–Consejo Superior de Investigaciones Científicas, Avda. de los Naranjos s/n, 46022 Valencia, Spain.

[‡] Packaging Lab, Instituto de Agroquímica y Tecnología de Alimentos, IATA–CSIC, Av. Agustín Escardino 7, 46980 Paterna, València, Spain.

[§] Departamento de Ciencia de Materiales e Ingeniería Metalúrgica y Química Inorgánica, Universidad de Cádiz, Campus Río San Pedro, Puerto Real, 11510 Cádiz, Spain.

◊These authors equally contributed to the work.

ABSTRACT: The assumption that oxidative addition is the key step during the cross-coupling reaction of aryl halides has led to the development of a plethora of increasingly complex metal catalysts, thereby obviating in many cases the exact influence of the base, which is the simplest, inexpensive and necessary reagent for this paramount transformation. Here, a combined experimental and computational study shows that the oxidative addition is not the single kinetically relevant step in different cross-coupling reactions catalyzed by subnanometer Pt or Pd species, since the reactivity control is shifted toward subtle changes in the base. The exposed metal atoms in the cluster cooperate to enable an extremely easy oxidative addition of the aryl halide, even chlorides, and allow the base to bifurcate the coupling. With subnanometer Pd species, amines drive to the Heck reaction, carbonate drives to the Sonogahira reaction, and phosphate drives to the Suzuki reaction, while for Pt clusters and single atoms, good conversion is only achieved using acetate as a base. This base-controlled orthogonal reactivity with ligand-free catalysts opens new avenues in the design of cross-coupling reactions in organic synthesis.

INTRODUCTION

Cross-coupling reactions of aryl halides are ubiquitous in modern synthetic chemistry, from research to industry.[1] In general, the rate-determining step (RDS) of the coupling reaction is the oxidative addition of the aryl halide on the metal, which is reflected in the typical reactivity order I > Br >> Cl. The following steps, i.e., transmetallation / alkene migratory insertion (for the Heck reaction) and reductive elimination, depend on the particular metal–organic reactant interaction that arises from the initial oxidative addition, and consequently, most efforts have focused on the design of organometallic species that are expected to collapse into the final coupling product. In contrast, the role of the base is usually overlooked, and it is commonly considered as a secondary player to capture released hydrogen atoms in a general way, although abstraction of the hydrogen atom out of the catalytic site is a fundamental part of the process. Taking into account that the base is the most reactive of the coupling reagents and is added in excess with respect to any other species, it seems reasonable to think that it could influence not only the overall reaction rate but also the selectivity of the process.

Ligand–free sub–nanometer Pd clusters are very active catalysts for cross-coupling reactions.[2] However, it has not been possible so far to assess the influence of the base on the reaction outcome, due to its excess in the reaction media and because the clusters are prepared and stabilized by acetate or amine bases in–situ, in reducing amide solvents. To address the action of the base during the coupling, without altering the catalyst, it is necessary to independently prepare the clusters (ex–situ) and add them to the reaction mixture. Here, we show that not only Pd but also Pt, subnanometer species of a few atoms can be prepared within ethylene vinyl alcohol co–polymer (EVOH) in a very simple, one–pot procedure to make stable and non–toxic (biocompatible) solid materials storable for at least 1 year. The solid–stabilized sub–nanometer Pd or Pt species catalyze the Heck, Suzuki and Sonogashira reactions of aryl halides, even chlorides, with simple inorganic bases, and experimental and computational evidence supports that the base that is employed directs the type of coupling to proceed. The fact that Pt, which traditionally has low activity as a catalyst for cross coupling reactions,[3] becomes active if prepared as a sub–nanometer species assisted by an appropriate base, illustrates the importance of atomicity in metal catalysts for cross coupling reactions, and brings Pt to the selected group of metals[4] that catalyze the Heck reaction by a recognizable redox mechanism.[5]

RESULTS AND DISCUSSION

Synthesis and characterization of sub–nanometer Pd and Pt species in EVOH.

The synthesis of Pd or Pt–containing EVOH co–polymers involves the dissolution of a small amount (typically 0.4 wt%) of

$Pd(OAc)_2$ or H_2PtCl_4 in the pre–polymeric hydroalcohol mixture with a stoichiometric amount of carvacrol as a reducing agent, and extrusion at 80 ºC (Figure 1a). EVOH co–polymers are semi–crystalline solids that are widely used in the food–packaging sector because they have outstanding oxygen barrier properties, chemical resistance and high transparency. In addition, the resulting, slightly yellow film of M@EVOH (M=Pd, Pt) contains a nominal amount of introduced metal, as assessed by inductively–coupled plasma mass spectrometry (ICP–MS) analysis of the metals extracted in isopropanol/water mixtures. In line with recently reported Cu or Au@EVOH,[6,7] infrared spectroscopy reveals the retention of crystallinity in the EVOH material after metal incorporation and that the hydroxyl groups present in the polymer can act as reducing agents for the noble metal salt (Figure S1 in Supporting Information). As also observed with Cu@EVOH,[6] the addition of carvacrol as an additional reducing agent is beneficial for further reduction of the Pd or Pt salt.

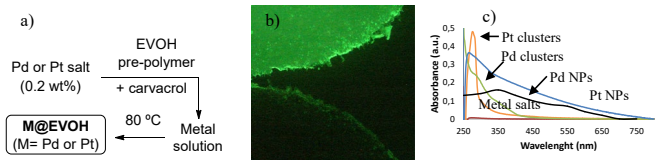

Figure 1. a) Synthesis of M@EVOH (M = Pd or Pt). b) Fluorescence microphotograph of Pt@EVOH (top) and EVOH (bottom). c) UV-vis absorption spectra of isopropanol/water Pd@EVOH (green line) and Pt@EVOH (orange line) extracts, metal salts (red line), cubo–octahedral Pt NPs of approximately 2 nm (blue line) and similar size Pd NPs (black line).

Figure 1b shows a representative fluorescence microphotograph of Pt@EVOH prepared without carvacrol to avoid emission signals of the organic compound (see also Figure S2). The formation of fluorescent compounds in the metal–containing film, clearly observed if compared to pristine EVOH, indicates the formation of sub–nanometer metal clusters, which present absorption and emission (fluorescence) properties in the ultraviolet–visible (UV vis) region, whereas when the Pd or Pt salts are employed, the corresponding nanoparticles (NPs) do not.

The sub–nanometer metal clusters can leach out from EVOH in diluted solutions, stabilized against aggregation by solvent molecules. The UV-vis absorption spectra of isopropanol/water extracts of Pd@EVOH (green line) and Pt@EVOH (orange line) in Figure 1c show clear bands at $\lambda<350$ nm, which are not observed in the UV-vis spectra of Pd and Pt salts (red line), independently prepared cubo–octahedral Pt NPs of ~2 nm (blue line) and Pd NPs of the same size (black line). According to the Jellium model, the 320–350 nm bands correspond to metal clusters of <5 atoms within the error range, and the UV-vis emission measurements after subtracting blank EVOH with carvacrol (Figure S3) confirm the fluorescent nature and sub–nanometer size of the absorbing species. Analysis by electrospray ionization with a time–of–flight mass detector (ESI–TOF, Figure S4) unambiguously shows, according to the isotopic pattern, that Pd clusters of less than 5 atoms (<600 Da) are the only species present in the isopropanol/water extracts of Pd@EVOH, with no heavier aggregates up to 1500 Da.

Dynamic light scattering (DLS) analysis of Pd@EVOH and Pt@EVOH extracts (Figure S5a, b) provides a radius of ~0.4–0.6 nm for the leached metal clusters, which fits well with an estimated atomicity of ~5 atoms or less,[2b] together with distribution curves for larger radii (1-3 nm). The appearance of distribution curves for larger radii (1-3 nm) is a physical property of the light scattering technique, in which the intensity of the light scattered is approximately the diameter to raised to the power 6, and given that this type of experiment considers the entire hydrodynamic radius, greater values might be as easily related to the solvated sub–nanometer clusters. The zeta potential of Pd@EVOH and Pt@EVOH extracts are nearly neutral (±6.0 mV, Figure S5b),[2b,6] in sharp contrast with Pd and cubo–octahedral Pt NPs that show a negative value of ~ -20 mV (Figure S5c). This agrees with the need of ultrasmall clusters to be stabilized by a number of strongly interacting solvent molecules in highly diluted solutions, much higher than NPs in comparative terms per metal atom; thus, the classical electrostatic stabilization of NP triggered by the potential surface is overridden by the stabilization with solvent molecules when the dilution is high enough, as is the case here. Notice that naked metal clusters in highly diluted solutions also present near-zero zeta potential values.[6]

Despite the difficulties associated with the measurement of a polymer in high-resolution microscope conditions, with potential burning of the samples, agglomeration of the supported metal species and contamination of the detectors by volatile carbonaceous substances, a spherical aberration corrected transmission electron microscope coupled to a high-angle annular dark field detector (HAADF-HRTEM) was used to analyze a sample of Pt@EVOH (0.2 wt% Pt) after gently depositing a sample of the solid dispersed in an organic solvent on the grid. After optimizing the recording conditions, the sample was stable enough to obtain some images, and the results obtained truly elucidate the nature of the Pt@EVOH catalyst. The images (Figures S6-8) show the concomitant presence of ultrasmall Pt clusters and <5 nm NPs with the remaining K and Cl atoms of the precursor K_2PtCl_4, as confirmed by energy-dispersive X-ray spectroscopy (EDS). It is difficult at this point to know whether or not the Pt NPs were generated during the preparation and analysis of the sample in the microscope. However, measurements from different times show the progressive formation of the NPs after prolonged exposure to the electronic beam. Very short time measurements, <1 min mainly show the subnanometer Pt species, which is in line with the characterization above and suggest that most of the observed Pt NPs are artifacts of the measurement. In any case, the predominant presence of subnanometer Pt clusters is clear.

All of the characterization data strongly support the reduction, aggregation and stabilization of sub–nanometer species of Pd and Pt within the EVOH structure. Some Pt NPs can originally be in the polymer, but their low abundance and lack of activity during the reaction compared to the subnanometer Pt species (see below) makes them mostly irrelevant for catalysis.

Heck reaction catalyzed by Pd clusters.

The Heck reaction of aryl iodides and bromides with acrylates is readily catalyzed by in–situ formed $Pd_{3–4}$ clusters after the endogenous reduction of Pd salts in aqueous amide solvents (DMF, NMP) at reaction temperatures >130 ºC.[2b] These reaction conditions are mandatory for the formation and activity of the tiny clusters, since the amide solvent reduces and aggregates the Pd compounds only at those temperatures,[8] with water as a cluster stabilizer.[4] These restrictions in the reaction conditions severely limit the application of the catalytic Pd clusters for other substrates and, for instance, styrenes are not reactive. In

the present work, the stabilization of Pd clusters in EVOH co-polymers allows us not only to use them on-demand as catalysts, as shown below but also to test other reaction conditions for Heck coupling. Thus, Figure 2 shows that styrenes can be coupled with different aryl iodides and bromides in toluene at 95 ºC, using dicyclohexyl methyl amine as a base, to produce the Heck products **A1**–**A7** with good to excellent yields and with selectivity toward the *trans* isomer. Acrylate also engages well during the coupling (product **A8**).

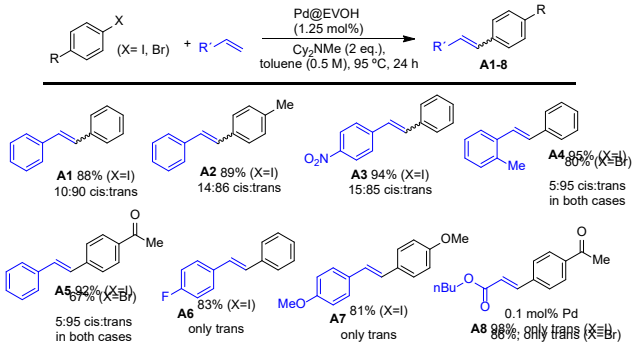

Figure 2. Results of the Heck cross–coupling reaction of different iodo- and bromoarenes with alkenes using Pd@EVOH as a catalyst and toluene as a solvent. Full conversion occurred in all cases, and the mass balance was completed with the corresponding biphenyl and benzene derivatives.

Kinetic experiments (Figure S9) do not show a visible induction period during coupling in toluene, which indicates that Pd@EVOH liberates the catalytically active sub–nanometer Pd clusters at the very beginning of the reaction. Notice that the activity of the Pd clusters is expected to occur in solution, since the clusters embedded within the polymeric framework are not accessible to reactants before their release. ICP–MS analysis of the EVOH polymer after the reaction confirms the complete liberation of the Pd cargo into solution. Nevertheless, a new experiment where Pd@EVOH is pre–dissolved with an isopropanol/water mixture before adding the reactants, which breaks the co–polymer crystallinity, shows a slightly faster initial rate than with Pd@EVOH directly. These results strongly suggest that Pd@EVOH can be used as a reservoir of sub–nanometer Pd clusters for the Heck reaction, to be liberated under the desired reaction conditions.

Heck reaction catalyzed by Pt clusters.

Pd and Ni compounds readily catalyze the Heck reaction, whereas the heavier element of group VIII, Pt, and any other metals, barely perform in the same manner.[4,5] To our knowledge, only some Pt salts and complexes dissolved in boiling amide solvents (DMF, NMP) have shown catalytic activity for Heck coupling,[7] and these reaction conditions are those in which very active, catalytic, sub–nanometer Pd clusters for cross–coupling reactions are formed, as explained before.[2b] Thus, it may very well be that Pt clusters are the active species for Heck coupling and, if suitably prepared, will efficiently catalyze the reaction.

Table 1 shows a variety of Pt compounds (2 mol%) that catalyze the Heck reaction between iodobenzene **A9** and butyl acrylate **A10** with KOAc as a base, in NMP at 135 ºC for 24 h. These include different Pt^{4+} (entries 1–3), Pt^{2+} (entries 4–8) and Pt NPs, which can be either supported or not and present different sizes and shapes (nanocubic, cubo–octahedral, quasi–spherical and irregular NPs, entries 9–14, see also Figure S10).[8] Pt chelates did not show better catalytic activity at lower temperatures (Table S1) or with other solvents (Table S2). All of the results provide lower yields than Pt@EVOH (93%, entry 15).

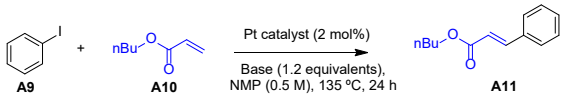

Table 1. Results for the Heck reaction catalyzed by different Pt compounds, calculated by gas chromatogram (GC) using *n*–dodecane as an external standard. Conversion refers to iodobenzene **A9**. Numbers in parentheses indicate isolated yields. The mass balance was completed with biphenyl and benzene.

Entry	Pt Catalyst	Base	Conversion (%)	A11 (%)
1	H_2PtCl_4	KOAc	100	76
2		Bu_3N	<5	-
3	$PtCl_4$ (≥99.99%)	KOAc	100	79(72)
4	$PtCl_2$	KOAc	100	75
5	$Pt(acac)_2$	KOAc	100	68
6		Bu_3N	<5	-
7	$Pt(NH_3)_4(NO_3)_2$	KOAc	100	84
8	$PtCl_2COD$	KOAc	100	65
9	Pt^{2+}–zeolite NaY	KOAc	100	86
10	Pt–C	KOAc	89	69
11		Bu_3N	<5	-
12	cubo–octahedral Pt NPs	KOAc	66	48
13	nanocubic Pt NPs	KOAc	60	42
14	irregular Pt NPs	KOAc	77	55
15	Pt@EVOH	KOAc	100	93(86)
16		Bu_3N	<5	-
17		K_2CO_3	15	14
18		K_3PO_4	30	27
19		KO^{t}Bu	<5	-
20		KF	<5	-
21		Cy_2NMe	25	22

Analogous to Pd@EVOH, ICP MS analysis confirmed the rapid deliverance of Pt clusters into solution from Pt@EVOH, and if the reaction is performed with Pt@EVOH pre–dissolved in an isopropanol/water mixture, a slightly faster initial rate is found. These results indicate that Pt@EVOH acts well as a reservoir of the catalytically active Pt species for the cross–coupling reaction, which are released under reaction conditions.

The presence of Pd impurities that could catalyze the reaction was evaluated by ICP–MS and the results showed that, in general, the tested Pt compounds contained <30 ppb of Pd. The remaining reagents, i.e., the organic substrates, KOAc and NMP, were also analyzed by ICP–MS after treatment with *aqua regia* and water extraction, and the results showed that the Pd content was <5 ppb. A sample of ultrapure $PtCl_4$ (entry 3) produced a good yield of **A11**, and when the reaction was performed in new glassware, similar results were obtained. Increasing amounts of $PdCl_2$ were added to the reaction system, up to 100 ppb, and neither the initial rate of the $PtCl_2$–catalyzed reaction (~30 h^{-1}) nor the final yield of **A11** (75%, entry 4) were significantly

modified.[9a] These results show that Pd traces are not responsible for the observed activity.

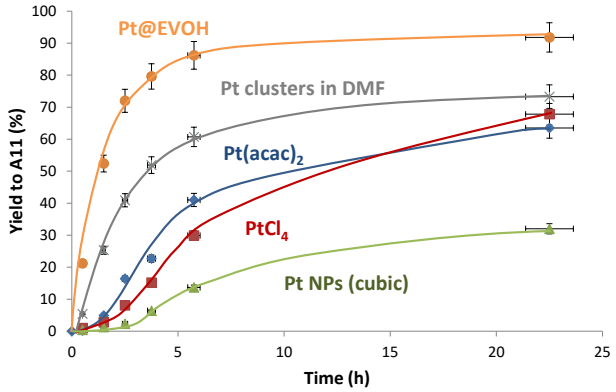

Figure 3. Kinetics for the Heck reaction shown in Table 1, catalyzed with 0.5 mol% of different Pt compounds. Error bars account for 5% uncertainty.

Figure 3 shows kinetic experiments for the Heck reaction with different Pt catalysts, and only Pt@EVOH presents a smooth kinetic profile with no induction time (orange line). $PtCl_4$ (Pt^{4+}), $Pt(acac)_2$ (Pt^{2+}) and Pt nanocubes (Pt^0) all produced sigmoidal curves with clear induction times. Hot filtration leaching tests together with ICP–MS analysis confirmed that all catalytic activity proceeds from the Pt species in solution.[9b,c] In addition, and only in the experiments with Pt salts, significant amounts of *N*–methyl succinimide (NMS), the oxidation product of NMP, were formed during the induction time. The formation of NMS is clearly indicative of the reduction of Pt at the expense of NMP oxidation, as it occurs for other metals.[10] The kinetic profile of sub–nanometer Pt clusters independently prepared in amide solvents[8] is very similar to Pt@EVOH, i.e., free of any induction time. Indeed, the kinetic curves show higher stability and activity of the Pt clusters if they are released from EVOH compared to when the clusters are formed in situ from Pt salts. These results suggest that sub–nanometer Pt clusters are the catalytically active species in the reaction, but it is not possible to completely discard the presence of some single atoms or Pt(0) species together with the clusters.

The induction time and the overall catalytic activity found for Pt NPs were longer and lower, respectively, than for the other catalysts. Since reduction cannot occur in this case, a dissolution/re–aggregation mechanism of Pt atoms can be operating for Pt NPs, as it occurs with Pd NPs.[2,11] To confirm this hypothesis, the course of the reaction with Pt NP catalysts was followed concomitantly by GC kinetics and UV vis emission spectrometry (Figure S11). This was done to determine whether and when the clusters are formed along the reaction. To avoid aromatic compounds and traces of soluble Pt species that could be emitted in the UV–vis region, the experiment was performed with 1–iodo–1–octene as the halide coupling partner and Pt–C as the solid catalyst. The results show that fluorescent, sub–nanometer Pt clusters are detected when the induction time of the reaction finishes and the coupling product starts to evolve. Thus, it seems that active clusters form in solution from Pt NPs.

To further confirm that sub–nanometer Pt species are the catalytically active species and that the EVOH polymer does not dissolve nor interfere during the reaction,[12] the Heck reaction catalyzed either by $PtCl_2$ or Pt@EVOH was also monitored by NMR and Fourier Transform Infrared (FT-IR) spectroscopy (Figures S12-S13). In the NMR experiments, deuterated DMF was used as solvent and 4–fluoroiodobenzene was chosen as a substrate to follow the reaction not only by ^1H but also by ^{19}F NMR spectroscopy. The results showed that the corresponding Heck product is visible for $PtCl_2$ after an induction time, in accordance with the kinetic curves, whereas for Pt@EVOH, the product forms progressively during the reaction (Figure S12). In addition, no EVOH residues are detected in the ^1H spectra, which indicates that the polymer is not dissolved under the reaction conditions and, apparently, does not interact with soluble catalytic Pt species. In the FT-IR studies (Figure S13), although DMF signals dominate the spectra, it is possible to observe the lack of peaks corresponding to EVOH polymer, which indicates that no EVOH monomers leach into the solution during the reaction, which is consistent with the NMR results.

The ability of EVOH to generate and stabilize the tiny clusters is further illustrated by the fact that Pt@EVOH prepared without carvacrol also catalyzes the reaction without any induction time (although at a lower rate), confirming that the EVOH structure alone can reduce the Pt salt and form the subnanometer species (Figure S14). Different EVOH compositions and curing methods including heat and UV light were tested, and most of the Pt@EVOH samples showed catalytic activity without induction time.

The reported data thus lead to the conclusion that the activity in all samples (Table 1) comes from sub–nanometer Pt species, formed from the reduction of Pt cations in the case of salts, and because of detachment in Pt NPs.

To check the stability and nature of the sub–nanometer Pt species during the reaction, we followed the Heck reaction in Table 1 with the Pt@EVOH catalyst by collecting periodic samples and quenching them in–situ with high-surface active carbon in order to trap the metal species. In this way, we concomitantly monitored the Pt species during the reaction using four different techniques: UV–Vis and fluorescence spectrophotometry for the liquid samples before quenching, and high–angle annular dark–field scanning electron microscopy (HAADF–STEM) and powder X-ray diffraction (XRD) for the supported Pt samples (Figures S15-17). First, absorbance and emission UV-Vis spectra of samples taken at 10, 20, 45 and 90 min reaction time show the presence of clusters of ~3-5 atoms from the beginning of reaction until the reaction rate decreases. At 9 h, when the reaction is finished, the fluorescence decays and the broad plasmon of Pt NPs begins to appear. These results suggest that Pt clusters, or at least subnanometer Pt species, are responsible for catalysis, and they finally aggregate into NPs when the reaction is finished. The sample impregnated on high surface area carbon at 90 min reaction time, after filtration and drying under a vacuum still shows mainly sub–nanometer Pt species in the HAADF–STEM images, whereas the sample at 9 h shows well-defined Pt NPs. The XRD results further support these findings, since typical diffraction values of Pt NPs arise for the samples after longer reaction times. This combined study confirms that the subnanometer Pt species responsible for catalysis stabilize in the presence of the reactants while the reaction proceeds and progressively aggregate into catalytically inactive NPs.

To clarify whether single-atom Pt species, together with metal clusters, are responsible for catalysis, $PtCl_4$ and $Pt(acac)_2$ were used as initial Pt sources and the Heck reaction was followed by UV-visible / fluorescence spectrophotometry and ultra-high pressure liquid chromatography–electrospray ionization mass–spectrometry (UPLC–ESI–MS) analyses. $PtCl_4$ forms clusters

during reaction, in accordance with the reported feasibility of noble metal cluster formation in the presence of chloride anions.[13] In contrast, $Pt(acac)_2$ generates single Pt atoms in NMP under basic conditions.[3d] The results show that both salts are reduced in less than 1 min under reaction conditions, since the corresponding absorption bands in the UV vis spectra disappear. However, while $PtCl_4$ aggregates into catalytically active $Pt_{3\text{-}5}$ clusters after the induction time and shows clear emission bands, $Pt(acac)_2$ does not show any emission corresponding to clusters event though it has good catalytic activity after a shorter induction time (see Figure 3 and Figures S18-S19). No plasmonic bands were found in the corresponding absorption spectra for $Pt(acac)_2$, and UPLC–ESI–MS detects peaks corresponding to Pt(acac) and $Pt(acac)_2$ species with no heavier aggregates. These results indicate that single Pt atoms are formed from $Pt(acac)_2$ and that they are catalytically active. When the highly coordinating ligand diphosphine (1,2-bis(diphenylphosphino)ethane (dppe, bite angle 86 º) was added at the first moment of the Heck reaction in Table 1, we observed that the reaction does not work for $Pt(acac)_2$ and $PtCl_4$ because the phosphine is coordinated so hard that both Pt cations hampered the reduction. When adding dppe after 20 minutes of reaction, the reaction curve suddenly stops for $Pt(acac)_2$ and continues growing for $PtCl_4$, nearly unaltered, with clear, fluorescent bands for clusters (Figure S20). These results strongly support that single Pt atoms are formed from $Pt(acac)_2$ and Pt clusters are formed from $PtCl_4$. If this is so, and in order to further compare the intrinsic catalytic activity of Pt single atoms and clusters, it may very well be that the clusters formed from $PtCl_4$ could act as seeds to incorporate the single Pt atoms from $Pt(acac)_2$, thus forming more catalytically active clusters. Indeed, the mixture of both Pt salts generates a large amount of clusters and, gratifyingly, shows that by adding just 0.2 mol% of $PtCl_4$ to a reaction with catalytic $Pt(acac)_2$, the TOF nearly triples (Figure S21 and Table S3). The opposite combination also works in that way, but produces smaller increases in the rate. It is noteworthy that the TOF is calculated based on the total Pt atoms, thus the TOF per cluster is much higher than the TOF per single atom in all cases. These results clearly show that Pt clusters are more active than single atoms and that the combination of $PtCl_4$ and $Pt(acac)_2$ generates a much more powerful catalyst. Following this rationale, the addition of Pt NPs to the medium should not produce any reaction rate increase and even reduce the catalytic activity of the subnanometer species after incorporation of the latter onto the former, which indeed occurs (Figure S22 and Table S3) and illustrates the need of having subnanometer species to catalyze the reaction.

All of the above strongly support that sub–nanometer Pt species, *both clusters and single atoms*, form under typical reaction conditions for the Heck reaction, regardless of the initial source of Pt employed and that the tiny Pt clusters are the true catalytically active species.[2,11]

Reaction mechanism of Heck coupling on Pd and Pt clusters.

Reactivity results. The accepted steps of the Heck reaction on organometallics include, in the following order, oxidative addition, alkene migratory insertion, *β*–hydride elimination and reductive elimination.[4] The uniqueness of the first group VIII transition metals, Ni and Pd, to catalyze the Heck reaction is a response to the need of articulating the intermediate steps at similar rates compared to the oxidative addition and reductive elimination steps. This is in contrast to other couplings where a transmetallation step circumvents the need for exclusively activating C atoms.

In principle, Pt^0 is amenable not only to alkene migratory insertion,[14] *β*–hydride elimination[15] and reductive elimination,[16] but also oxidative addition of the C_{sp2}–halide bond.[17,18] The latter is generally the RDS of the reaction, and has been unambiguously snapshotted with a variety of single-atom, heavy–late organometallic complexes of Pt and Au.[17,18] However, kinetics for different sub–nanometer cluster catalysts and reagent concentrations at initial reaction times show that the rate equation is $v_0 = k_{app1}[Pd][PhBr][KOAc][acrylate]^{-1}$ and $v_0 = k_{app2}[Pt][PhI][KOAc][acrylate]$ for Pd and Pt clusters, respectively, which indicates that all of the reagents are implicated in the RDS of the reaction (Figures S23-24), including those that are base-employed. It must be noted that the [base] is irrelevant at high concentrations (>0.5 M), and this rapid saturation of the catalytic site may also explain why the amount and nature of the base has traditionally been obviated from mechanistic studies.

After the observation that the base appears to affect the reaction according to this kinetic data, a second observation of Table 1 reveals that the activity of Pt clusters is dramatically lost when employing Bu_3N. Furthermore, KOAc as base is needed to produce good conversion, although all bases provide good selectivity to the Heck product. This effect does not occur for the Pd clusters,[2b] where amines and other inorganic bases are also active. Kinetic measurements made by changing the cation to increase the basicity of the acetate (from Li^+ to Cs^+) do not show any significant influence in the initial rate of the reaction with Pt clusters (Figure S25). This, together with the fact that carbonates and phosphates of higher pK_a (between 9 and 12) are not effective either,[19] indicates that intermolecular deprotonation based on classical acid–base interactions (in what would be the last reductive elimination of the Heck reaction) is not the main effect of the base and does not explain why only KOAc is effective. The possible dual base/stabilizer role of KOAc was also discarded by kinetic experiments where acetyl acetate, AcOAc, is added to Bu_3N to mimic the effect, which provided unsuccessful results similar to Pt clusters (Figure S26). Lastly, the acetate is a prototypical ambiphilic base,[20] and a chelating effect has been previously observed in C-H activation reactions promoted by bimetallic molecular complexes.[21] Thus, the possible interaction of the acetate with different Pt atoms of the cluster seems reasonable to explain the uniqueness of this base to trigger the Pt–catalyzed Heck reaction.

From the results above, it is clear that the reaction mechanism of Heck coupling on Pd or Pt clusters is not straightforward. To identify the differences between the metals and determine the mechanism, the four elemental steps of the traditional Heck reaction were studied by means of DFT calculations on Pd_3 and Pt_3 cluster models.

Theoretical study of the mechanism of Heck coupling on Pd and Pt clusters.

Oxidative addition of iodobenzene. Figure 4 shows that the most stable structure for the adsorption of the reactant iodobenzene is different in each cluster. For palladium, iodobenzene is preferentially adsorbed through the arene, face to face with the three metallic atoms, whereas for platinum, adsorption occurs on the edge of the cluster, either through the cycle or along the C-I bond.

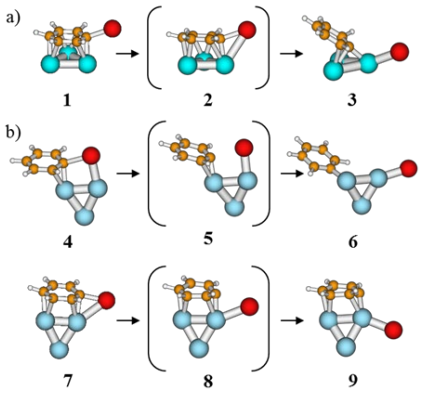

Figure 4. DFT-optimized structures for the oxidative addition of iodobenzene to Pd_3 (a) and Pt_3 (b) clusters.

Figure 5 shows that this difference in adsorption is readily explained by the shape of the HOMO and LUMO of each cluster. The interaction involves a charge transfer from the HOMO of the metal cluster to the LUMO of iodobenzene (σ*(C-I), centered along the C-I bond) and back-bonding from the LUMO of the cluster to the HOMO of the molecule (characterized by a mixture of the p_z orbital of the I atom and π contributions from the ring).[22] The LUMO of Pd_3 is lower-energy, which enhances the back-bonding interaction and is spread in the face of the cluster, hence matching the HOMO of iodobenzene and directing the adsorption of the molecule through the cycle toward this face. In spite of this, the adsorption energy is ultimately higher for Pt_3, presumably due to the rupture of the aromaticity in the benzene ring of iodobenzene after planar adsorption on Pd_3.

Other minima close in energy to **1** and **4** can be observed for both clusters (see Figure S27). However, it is notable that although the same stable adsorptions along the edge of Pd_3 are found for Pt_3 (structures **S1** and **S2** in Figure S27, approximately 5 kcal/mol higher in energy), the structure analogous to **1** with iodobenzene in the face of a Pt_3 cluster is almost 26 kcal/mol less stable (structure **S24**). Table 2 shows, surprisingly, very low activation energies for this elementary step for both clusters: as low as 0.6 and 2.5 kcal/mol for Pd_3 and Pt_3, respectively. The imaginary mode of transition state (TS) **2** involves the displacement of the molecule in the face of the cluster, but as soon as the iodine touches the palladium in this structure, the molecule dissociates; no intermediate could be stabilized prior to **3** and no other TS more clearly showed the breaking of the C-I bond. Alternative paths from the close energy minima similarly produce very low barriers (Figure S28). The highest barrier of 9 kcal/mol is found for structure **7** of Pt_3, which is practically isoenergetic with structure **4**, but on which the breaking of the C-I bond takes place at the corner of one platinum atom instead of between two platinum atoms. In addition, the process is thermodynamically favored for both Pd_3 and Pt_3. Therefore, oxidative addition proceeds with ease in both clusters, but even more so in Pd_3.

The oxidative addition step was also calculated for $PdCl_2$ and $PtCl_2$ to model the reactivity of Pd^{2+} and Pt^{2+} cations, as well as for reduced Pd_1 and Pt_1 single atoms (Figure S29). The activation barriers on $PdCl_2$ and $PtCl_2$ are > 10 kcal/mol higher than on the corresponding reduced atoms, which in turn are ~3 kcal/mol higher than on Pd_3 and Pt_3 clusters. These values suggest that although single atoms cannot be excluded as catalytic species, their reactivity is not higher than that of small clusters, which is consistent with the previously described experiments with $Pt(acac)_2$.

Consistent these data, a Hammett plot for different experiments with aryl iodides and *n*–butyl acrylate with Pt clusters (Figure S30) gives a ρ value of +1.5, which is an intermediate value between the typical value for Pd (+2.3)[23] and Cu (+0.5).[24]

Table 2. DFT-calculated electronic adsorption energies of the reactants, $\Delta E_{ads}(R)$, activation energies, ΔE_{act}, and electronic reaction energies, ΔE_{reac}, for the elemental steps shown in Figures 4-8 (in kcal mol^{-1}). Corresponding Gibbs free energies are provided in Table S4.

Path	Catalyst	$\Delta E_{ads}(R)$	ΔE_{act}	ΔE_{reac}
Oxidative addition				
1-[2]-3	Pd_3	-35.7	0.6 (2.2[a])	-26.1 (-14.2[a])
4-[5]-6	Pt_3	-49.6	2.5 (5.1[a])	-21.3 (-11.[a])
7-[8]-9		-50.0	9.1	-5.8
Alkene insertion				
11-[12]-13	Pd_3	-36.3	30.2 (18.8[a])	-3.4 (-11.6[a])
15-[16]-17	Pt_3	-62.7	44.8 (27.2[a])	23.3 (-3.4[a])
β-elimination				
18-[19]-20	Pd_3	-	6.9	-12.7
21-[22]-23	Pt_3	-	3.9	-22.6
Reductive elimination with KOAc				
24-[25]-26	Pd_3	-	29.2	19.9
27-[28]-29	Pt_3	-	27.9	17.2
Reductive elimination with NMe_3				
30-[31]-32	Pd_3	-23.4	28.8	28.4
33-[34]-35	Pt_3	-44.1	40.6	28.7

[a] For the same paths including a coadsorbed solvent molecule (Figures S32 and S33).

Alkene migratory insertion and β-elimination. Figure 6 shows the study of the alkene migratory insertion step, starting by coadsorption of *n*-butyl-acrylate with the most stable product intermediates from the previous step. Adsorption structures in which the acrylate only interacts through the double bond are found to be less-stable than those where oxygen atoms also participate (Figure S31a). Other more stable initial structures, by 9.4 and 7.2 kcal mol^{-1}, were respectively found for Pd_3 and Pt_3 (structures **10** and **14** in Figure 6), but the associated barriers were too high (more than 50 kcal mol^{-1}) and are not shown. The minima and the transition states of this step are similar in both metal clusters, and in the TS, the acrylate moves toward the adsorbed phenyl and the interaction of its oxygen atoms is lost. As a result, the alkene insertion is a difficult process in the two systems, and again is more difficult for Pt_3 than Pd_3 (see Table 2).

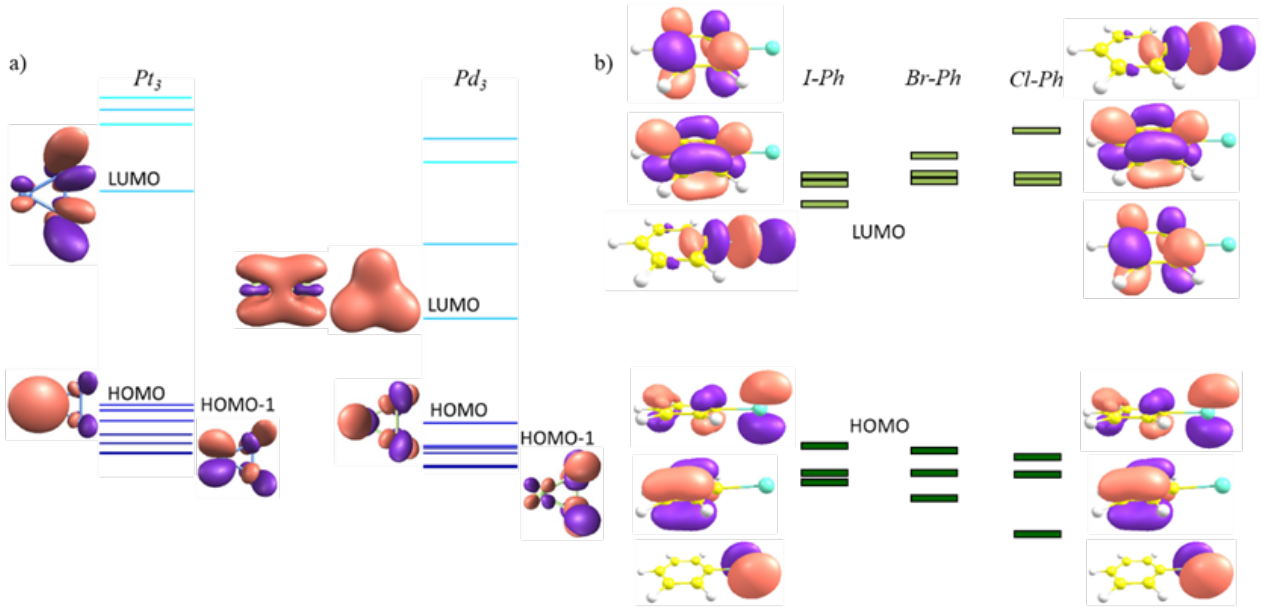

Figure 5. Molecular orbital distribution and composition of the highest occupied and lowest unoccupied molecular orbitals of a) Pt_3 and Pd_3 clusters calculated at the B3LYP/LANL2DZ level and b) Iodo-, Bromo- and Chlorobenzene adapted from ref. 22.

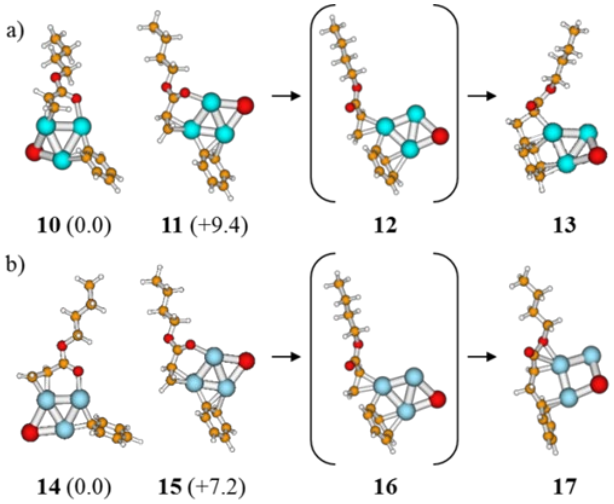

Figure 6. DFT-optimized structures for the alkene insertion of iodobenzene into Pd_3 (a) and Pt_3 (b) clusters.

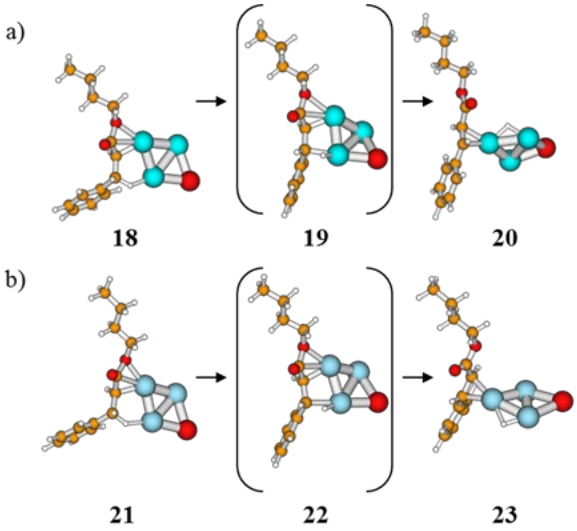

Figure 7. DFT-optimized structures for the *β*-elimination step for Pd_3 (a) and Pt_3 (b) clusters.

Then, the *β*-elimination step generates the final product, as shown in Figure 7. The abstraction of the hydrogen atom closest to the metal catalyst very clearly leads to the *trans* product isomer, but this stereospecificity is derived from the previous adsorption mode of the *n*-butyl-acrylate to the metal. Indeed, the fact that minima are more stable when one of the oxygen atoms of the molecule also participates in the adsorption causes a steric impediment for any molecule that is derived from the *cis* side. Adsorption of a styrene molecule on the cluster (Figure S31c) shows that this must also be the case for styrenes, as the participation of the aromatic ring in the adsorption also stabilizes the system. As a result, in the coupling step, the adsorbed phenyl always prefers the opposite side of the adsorbed double bond, thus leading to the *trans* product isomer that is consistent with the experiment.

Reductive elimination. The final step of the coupling is the recovery of the clean cluster catalyst in order to start a new cycle, which is achieved through a reductive elimination step by reaction with a base. Figure 8 models both acetate and trimethylamine (NMe_3, as a simplified model representative of Bu_3N), as the greatest differential behavior between Pt_3 and Pd_3 lies in the inactivity of the former with Bu_3N. Note that in the case of the acetate, the iodine anion is removed, assuming its reaction with the K^+ cation.

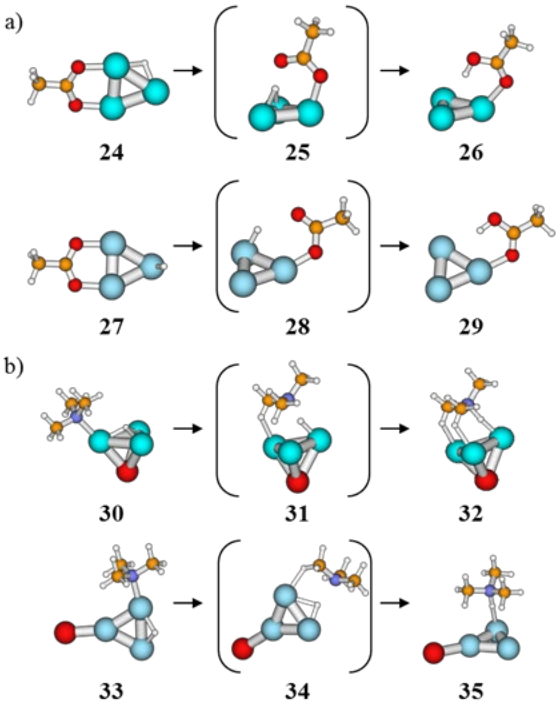

Figure 8. DFT-optimized structures for the reductive elimination step with acetate (a) and trimethylamine (b) for Pd_3 (top) and Pt_3 (bottom) clusters.

The acetate adsorbs on the metal cluster through the two oxygen atoms, whereas trimethylamine produces a single interaction through its nitrogen atom. This step constitutes a difficult process for the two bases in both metal clusters, but a 10 kcal mol^{-1} higher barrier is obtained for Pt_3 with NMe_3 (see Table 2). The difference in these processes for the two metals lies in the increased adsorption of trimethylamine on the Pt_3HI intermediate compared to that on Pd_3HI. Indeed, hydrogen and iodine preferentially adsorb into the facets of the palladium cluster, which leaves all metal atoms more coordinated than in platinum. Thus, although adsorption energies of reactants are consistently higher on Pt_3 (see Table 2 and Figures S26, S31), the adsorption energy of NMe_3 further increases by 6 kcal mol^{-1} when going from clean Pt_3 to Pt_3HI. In the case of palladium, the adsorption energy additionally decreases when going from the analogous Pd_3 to Pd_3HI (by 2 kcal mol^{-1}). In the case of acetate, the transition state does not require complete desorption of the base in either system, and similar barriers are produced for the two metals. Note that the consistently higher adsorption energy for platinum is nevertheless also observed when evaluating the adsorption of the resulting acetic acid, which is 13 kcal mol^{-1} more stable than Pt_3 (-33.0 vs -19.9).

Proposed mechanism.

The surprising differences in the barriers for the first two elementary steps on the small clusters, with respect to what is traditionally found for organometallics and with the oxidative addition not being the RDS of the reaction, seem to be caused by the metallic nature of the catalytically active species and by the additional participation of more than one metal atom in the process. Thus, while this produces the desired easier breaking of the C-I bond of iodobenzene, it also allows a higher stabilization of the fragments for the subsequent coupling. As a consequence, higher activation barriers are obtained for the alkene coupling step. However, note that the inclusion of only one molecule of each pertinent reactant in our model neglects the effect that the coadsorption of other reactant or solvent molecules can have in the reaction. Indeed, it is reasonable that additional adsorbed molecules may favor recombination steps and may impede bond-breaking reactions. Furthermore, the relatively large adsorption energies of all reactants in both catalysts (Figures S27 and S31) support the model of clusters surrounded by interacting molecules. With this in mind, we also simulated the oxidative addition and the alkene insertion steps with one solvent molecule of NMP adsorbed in the cluster (Figures S32 and S33). The influence of one coadsorbed solvent molecule on the oxidative addition step is limited, since activation energy barriers only increase from 0.6 to 2.2 kcal mol^{-1} for Pd_3 and from 2.5 to 5.1 kcal mol^{-1} for Pt_3. In contrast, the high barrier corresponding to the alkene coupling decreases by more than 10 kcal mol^{-1} in both catalysts as soon as another molecule impedes the enhanced stabilization of the acrylate through its oxygen atoms. Consequently, with the data presented here, it is concluded that i) the oxidative addition is not the RDS of the reaction, ii) the *β*-elimination is not a complicated process on either cluster, and iii) both the alkene insertion and the final reductive elimination steps are two difficult processes for both Pt_3 and Pd_3 clusters. It is therefore not surprising that the rate of the reaction depends on what gives rise to the coupling parts of the alkene insertion, namely, [PhI] and [acrylate], and on the base, [KOAc].

Following the comparison of platinum and palladium, Figure 9 shows that while the mechanisms are similar for Pt_3 and Pd_3 clusters, alkene insertion and reductive elimination by trimethylamine are particularly problematic for platinum (see Table 2). In both cases, the key issue seems to be the enhanced adsorption of reactants with Pt_3. If the structures and adsorption energies of all reactants on clean clusters are compared (Figures S27 and S31), it is clear that iodobenzene and *n*-butyl acrylate generally interact with two atoms of the cluster. Thus, the comparable structures with two molecules of NMe_3 provide larger adsorption energies in the case of Pt_3 by at least 10 kcal mol^{-1}. The values are, however, much closer for all adsorbates in Pd_3, hence suggesting poisoning by NMe_3 of the Pt_3 catalyst. This idea is consistent with Cy_2NMe providing some activity, as its cyclohexyl groups would serve as both stabilizing agents of the molecule when desorbing to react and steric impediments to adsorb two molecules of base in close Pt atoms. Indeed, since all reagents bind more strongly to Pt_3, the interaction of the cluster with the base needs to be strong enough to displace one of the adsorbed reagents near the adsorbed hydrogen atoms. However, it should not be too strong, or it would not be able to desorb and react. In such a situation, maintaining a certain degree of stabilization of the base during the reaction would greatly facilitate the process, which was observed for acetate, in which one oxygen atom binds the molecule to the cluster while the other interacts with the hydrogen atom. Although inconclusive, these results indicate that too strong adsorption of the base may be the general cause for deactivation in Pt_3 and that the combined effect of adsorption and stabilizing (chelating) interactions of KOAc with the cluster are the key to catalyze the Heck reaction in this system. Pd_3, in contrast, would not have any problem with the majority of bases because the adsorption energies of all reagents are similar or lower. This, in addition, would also explain the fact that higher concentrations of the acrylate also decrease the catalytic activity, for they would occupy the active sites and impede the adsorption and reaction of the base. In Pt_3, the bases seem to be the more strongly adsorbed species, and a

higher concentration of the acrylate only favors the difficult alkene migration step and leads to a higher rate of the reaction.

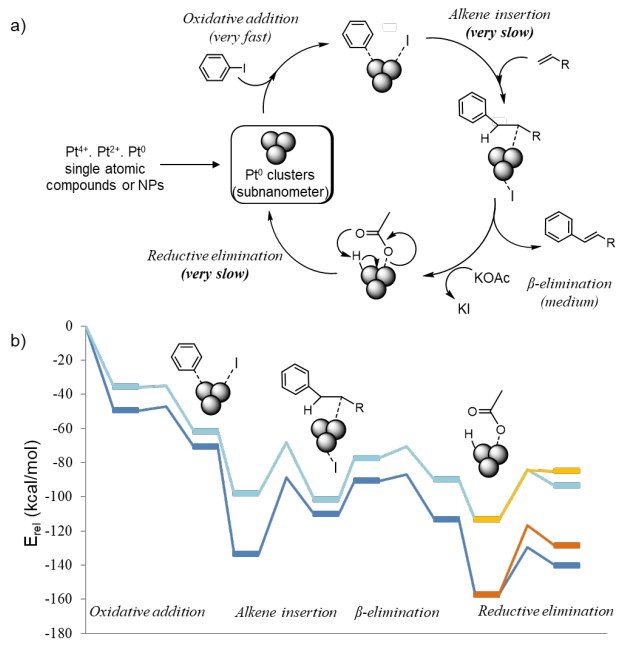

Figure 9. Proposed mechanism for the Heck reaction catalyzed by sub–nanometer Pt clusters (a) and free energy profile for the reaction mechanisms explored for Pd_3 (light blue) and Pt_3 (dark blue) using KOAc as a base (b). Yellow and orange lines correspond to the reductive elimination by NMe_3 in Pd_3 and Pt_3, respectively. Minima are indicated by rectangles. The adsorption energy of OAc is unknown and its reductive elimination step was aligned with that of NMe_3.

Figure 9a depicts the proposed mechanism for the Heck reaction catalyzed by sub–nanometer Pt clusters, taking into account all abovementioned considerations. The mechanism for Pd clusters would be analogous, but extendable to other bases.

Oxidative addition of bromobenzene and chlorobenzene. Taking into account the low energy barriers obtained for the oxidative addition of iodobenzene on the two clusters, as well as the fact that the Heck reaction with bromoarenes also occurs with palladium, we theoretically investigated the oxidative addition of bromobenzene and chlorobenzene to Pd_3 and Pt_3 clusters (see Figure 10). Table 3 shows that the interaction strength, and thus the adsorption energy, of the molecules slightly decrease from iodobenzene to bromobenzene and to chlorobenzene (see also Table 2). In addition, in Pt_3 a structure analogous to **4** for bromobenzene and chlorobenzene becomes more unstable, much more for the latter (+6.0 and +10.7 kcal/mol, respectively, see Figure S27). Both observations are again explained by investigating the HOMO and LUMO orbitals of each molecule (see Figure 5). Indeed, while their HOMO levels (characterized by the p_z orbital of the heteroatom and π contributions from the aromatic ring as mentioned before) are similar, the σ*(C-X) LUMO increases in energy, weakening the back-bonding interaction with the metal. Moreover, it changes in nature. Thus,

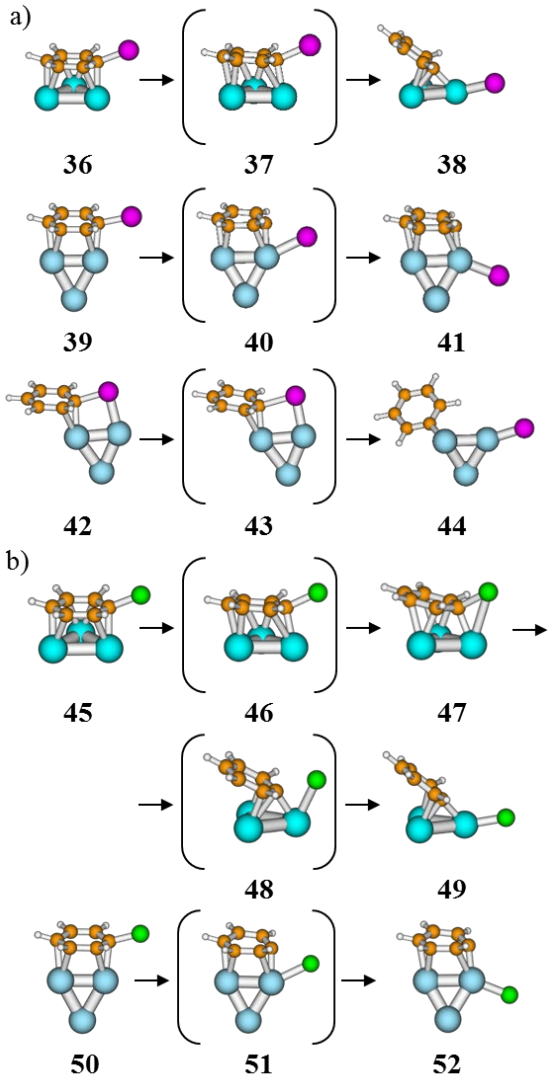

Figure 10. DFT-optimized structures for the oxidative addition of bromobenzene (a, Br in magenta) and chlorobenzene (b, Cl in green) on Pd_3 (top) and Pt_3 (bottom) clusters.

the σ*(C-X) orbital becomes increasingly destabilized in bromobenzene and more specifically in chlorobenzene, for which an aromatic π* orbital becomes the LUMO.[22] As a result, in going from iodobenzene to chlorobenzene, the interaction is increasingly stabilized when the molecule is adsorbed through the cycle.

While the activation energies for this elemental step follow the expected order according to the C-X bond strength, i.e., that of iodobenzene is lower than bromobenzene (which is also lower than that of chlorobenzene), activation energies are still strikingly low, especially that of Pd_3 (see Table 3). In the case of chlorobenzene on Pd_3, the increased strength of the C-X bond allows for stabilizing an additional reaction intermediate and a transition state where the breaking of the bond is clearer. Indeed, after a transition state **46** fully analogous to **2** and **37**, an intermediate structure with a bent chlorobenzene is found (**47**), whose C-Cl bond breaks through a transition state, **48**, that provides the highest barrier (4,3 kcal mol^{-1}). The fact that both structures **47** and **48** are more stable than initial reactant **45**, and the reasonable presumption of an analogous but lower barrier in

Table 3. DFT-calculated electronic adsorption energies of the reactants, $\Delta E_{ads}(R)$, activation energies, ΔE_{act}, and electronic reaction energies, ΔE_{reac}, for the oxidative addition of bromobenzene and chlorobenzene shown in Figure 10 (in kcal mol^{-1}).

Path	Catalyst	$\Delta E_{ads}(R)$	ΔE_{act}	ΔE_{reac}
Oxidative addition of PhBr				
36-[37]-38	Pd_3	-34.2	+1.4	-22.8
39-[40]-41	Pt_3	-46.6	+14.5	-3.8
42-[43]-44		-40.6	+1.8	-24.7
Oxidative addition of PhCl				
45-[46]-47	Pd_3	-33.1	+2.2	-4.8
47-[48]-49		-	+4.3	-13.2
50-[51]-52	Pt_3	-45.4	+22.4	+0.6

the case of iodobenzene and bromobenzene, explains why the optimization of the structures always leads to structures **3** and **38**, respectively.

For Pt_3, transition states **40** and **51** are analogous to **8**, whereas TS **43** is analogous to **5**. The oxidative addition of chlorobenzene on Pt_3 is neither kinetically nor thermodynamically favored. However, in the case of bromobenzene, although structure **42** is 6.0 kcal mol^{-1} higher than structure **39** in energy, it also provides a much lower barrier of only 1.8 kcal mol^{-1} (7.8 from the most stable minimum). Therefore, although barriers are higher on Pt_3 with respect to Pd_3, according to these results, the oxidative addition could also be possible for bromobenzene on Pt_3.

Figure 11 shows that Pt@EVOH experimentally catalyzes the Heck reaction not only for different aryl iodides but also for aryl bromides with alkenes in the presence of KOAc. Aryl iodides react well with acrylates and styrene to produce good to excellent yields of the coupled products **A5–A15**, including the industrially produced UV–protecting agent cinnamyl **A16**. Aryl bromides are also reactive and produce the same products, but with lower yields. It must be noted that EVOH and Au@EVOH[12] cannot perform the Heck coupling at all with any haloarene, in contrast to Pt@EVOH and that the reaction yields of the desired products are also dependent on the type of substituents, even though the oxidative addition is not the only RDS.

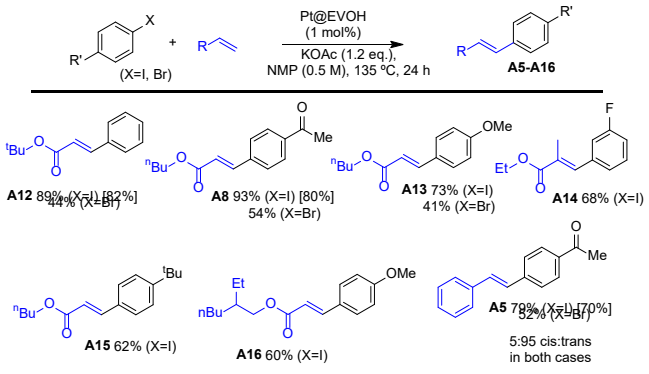

Figure 11. Results of the Heck cross–coupling reaction of different iodo- and bromoarenes with alkenes using Pt@EVOH as a catalyst. GC yields, between brackets isolated yields. For full conversion of aryl iodides, mass balance completes with biphenyl and benzene derivatives. For aryl bromides, a 20% of biphenyl and benzene derivatives is typical.

In summary, the oxidative addition does not limit the Heck reaction for neither clustered nor single atoms and that the chosen base has a larger impact on reactivity than was traditionally thought. These results lead us to think that the base may ultimately control the result of not only the Heck reaction but also other cross–coupling reactions on both Pt and Pd subnanometer catalysts.

Base–controlled Heck, Suzuki and Sonogashira reactions catalyzed by Pt@EVOH and Pd@EVOH.

Table 4 shows competitive reaction experiments for the Heck, Suzuki and Sonogashira reactions catalyzed by Pt@EVOH and Pd@EVOH in the presence of different bases (see Table S5 for non–competitive experiments and Figure S34 for a more visual representation).

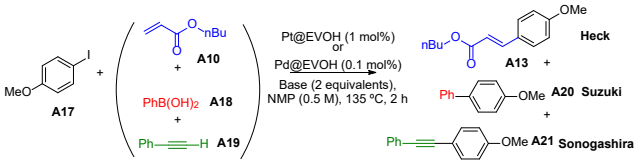

Table 4. Results for the Heck, Suzuki and Sonogashira reactions catalyzed by either Pd or Pt@EVOH in the presence of different bases, in NMP (0.5 M) at 135 ºC for 2 h. Yields are calculated by GC using *n*–dodecane as an external standard. Conversion refers to **A17**. Mass balance is completed with biphenyls and anisole.

Entry	Catalyst	Base	Conversion (%)	Yield to A13/A20/A21 (%)[b]	TOF_0 A13/A20/A21 (h^{-1})
1[a]	Pt	KOAc	64	28/-/33	20 /- /26
2	Pd		100	**57(51)**/-/38	**430**/-/210
3[a]	Pt	K_3PO_4	42	7/-/34	4/-/22
4	Pd		100	32/**59(56)**/3	190/**530**/20
5	Pt	K_2CO_3	38	3/-/33	-/-/19
6	Pd		100	36/6/**51(39)**	310/45/**420**
7	Pt	Bu_3N	<5	-/-/-	-/-/-
8	Pd		100	**91(78)**/-/5	**1200**/-/41
9[a]	Pd	Cy_2NMe	100	**99(92)**/-/-	**1325**/-/-

[a] Same results with Pd_{3-4} clusters formed in situ, see Ref. 2b. [b] Isolated yields are listed between parentheses.

For Pt, KOAc is still the only base that enables the Heck reaction between iodoanisole **A17** and *n*-butylacrylate **A10** to arene **A18** (entry 1), whereas the Sonogashira reaction with phenylacetylene **A19** (entries 3 and 5, product **A21**) proceeds with KOAc, K_3PO_4 and K_2CO_3, for which the greatest conversion is obtained with KOAc. Bu_3N is completely inactive, and the Suzuki reaction is not preferential in any case, only providing a good yield of product **A20** in the individual reaction with K_2CO_3 (entry 6 of Table S5).

For Pd, the Heck coupling in the presence of amine bases proceeds without significant amounts of Suzuki or Sonogahira products (entries 8 and 9), with KOAc also favoring the Heck

product to a lesser extent (entry 2).[2b] $Pd_{3–4}$ clusters that formed through the endogenous reduction of $Pd(OAc)_2$ in aqueous NMP[2] show a similar reactivity to Pd@EVOH, strongly supporting the catalytic action of Pd clusters released from the film. K_3PO_4 leads to a dramatic increase in the formation of the Suzuki product **A20** (entry 4) and K_2CO_3 causes a substantial increase in the formation of the Sonogashira product **A21** (entry 6) with the Pd@EVOH catalyst. Note that these bases are not suitable for generating soluble Pd clusters in–situ from the endogenous reduction of Pd salts,[2b] and thus Pd@EVOH has unveiled the true reactivity of K_3PO_4 and K_2CO_3 in the couplings. The success in the Suzuki reaction with Pd@EVOH further confirms the absence of Pd impurities in Pt@EVOH, which does not work under similar reaction conditions. In general, the use of Pt and Pd chelate complexes and NPs provided much poorer results, although with similar trends regarding the action of the base (Tables S6–7 and Figures S35–36).

With the complete description of the kinetic parameters of the Heck reaction and the effect of the base, we tried to further optimize the synthesis of the industrially produced UV–protecting agent **A16**. Since the reaction under stoichiometric conditions was inversely proportional to the alkene concentration (see equation rate above), we optimized the synthesis by changing the initial concentrations of both alkene and bromoanisole (([Pd] = 0.0005 M, Figure S37). Afterward, we slowly added the alkene along the reaction until it reached 1 equivalent, in order to maintain the highest catalytic activity during the reaction. In this way, the reaction proceed smoothly and faster than before, reaching 97% yield after 4 h (Figure S38). This is a large difference compared to the stoichiometric reaction and the one-time addition of the alkene at the beginning.

The different results show that the starting bromo- and chloroarenes are converted to 10-20% of the homocoupling product and another 5-10% of benzene derivatives when the coupling reactions are not extremely fast. Theoretical studies show that the activation energy barrier for the homocoupling is affordable for both metal clusters (Figure S39). Requiring the coadsorption of two identical molecules in the same catalytic site, together with enhanced adsorption of the *n*-butyl-acrylate after the oxidative addition of one aryl halide molecule, justifies the lower rate of the homocoupling reaction with respect to the desired cross-coupling.

Together, these results indicate that a judicious choice of the base maximizes a particular cross–coupling reaction with the sub–nanometer metal catalysts, for both Pt and Pd. While the theoretical results on KOAc and NMe_3 presented herein are indeed illustrative of this fact, further calculations on the complete and competitive reaction mechanisms of the Sonogashira and Suzuki reactions are necessary to precisely state the specific roles of each of the bases in facilitating one reaction over the other.[25] Nevertheless, in accordance with the ease of overcoming of the energy barrier that was computationally determined for the oxidative addition of chlorobenzene by the Pd single atoms and clusters, Figure 12 shows that the Suzuki coupling of aryl chlorides with different boronic acids proceeds well with Pd@EVOH and K_3PO_4 as a base, to yield the coupling products **A22-A28**. These reaction protocols constitute a rare case of ligand-free metal activation of aryl chlorides for Suzuki cross-coupling reactions.

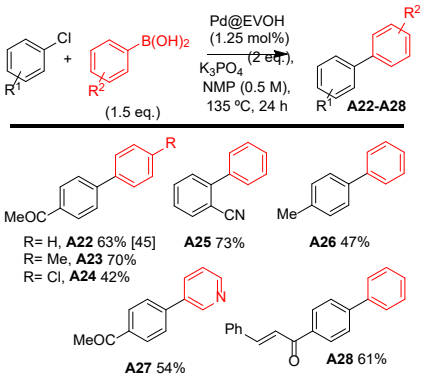

Figure 12. Results for the Heck cross–coupling reaction of aryl chlorides and phenyl boronic acids using Pd@EVOH as a catalyst and K_3PO_4 as a base. GC yields; isolated yields are reported between brackets. The corresponding biphenyl and benzene derivatives of the aryl halides were found as byproducts in minor amounts (<20%).

CONCLUSIONS

The Heck, Suzuki or Sonogashira cross–coupling reactions are selectively catalyzed by sub–nanometer Pd as well as Pt clusters with <5 atoms, depending on the base employed. The clusters were prepared within EVOH co–polymer films and were liberated under demand in the required reaction media, which allows unveiling the particular reactivity of the bases in different solvents. A combined experimental and computational study shows that the base–controlling effect arises from overcoming the energetic barrier of the oxidative addition and translating the RDS of the coupling to a later step where the base actively participates. Indeed, computational calculations indicate that an adequate balance of the adsorption strength of the base and its ability to undergo the reductive elimination step is key to catalyzing the Heck reaction. With a suitable base, the ligand–free Pt–catalyzed Heck coupling of aryl iodides and bromides, as well as the Pd–catalyzed Suzuki coupling of aryl chlorides, could successfully be performed, bringing Pt into the selected group of well–defined metals that can be used as catalysts for the Heck reaction. These results open the possibility of designing future cross-coupling reactions-based not only on the catalyst but also on the base.

EXPERIMENTAL SECTION

Preparation of M@EVOH (M=Pd or Pt). Pellets (2 mm diameter, 3 mm long) of EVOH with ethylene molar contents of 26 (EVOH26), 29 (EVOH29), 32 (EVOH32) and 44 (EVOH44) were supplied by The Nippon Chemical Company (Osaka, Japan). 13 g of EVOH29 were initially dissolved in 100 mL of a 1:1 (v:v) 1–propanol:distilled water mixture that was heated at 75 ˚C under reflux. Once the copolymer was completely dissolved, the mixture was left to cool to room temperature, after which $PdOAc_2$ or H_2PtCl_4 were added in order to obtain a metal loading of 0.02 mmol M/g dry polymer. The resultant suspension was spread on a Teflon-coated glass plate using a 200 µm spiral bar coater. A digital Mitutoyo micrometer (Metrotec, San Sebastian, Spain) was used to determine film thickness, with an average value of 0.012± 0.003 mm.

To evaluate the influence of film thickness, the ethylene molar percentage of EVOH as well as the influence of UV radiation

of the film in the formation of M clusters of different materials were obtained. To obtain thicker films, a 100 µm spiral bar coater was also used to provide films with 0.022 ± 0.004 mm of thickness. To check the effect of copolymer composition, films based on three EVOH precursors (EVOH26, EVOH32 and EVOH44) were also prepared using the same procedure. To determine the effect of radiation on cluster formation in the films, M@EVOH films were exposed to the radiation of a Heraeus NIQ 80/36U lamp at 5-cm distance for 15 min.

Typical procedure for cross–coupling reactions catalyzed by M@EVOH (M= Pd or Pt). The EVOH film (typically 44 mg, 1 mol% in metal for the reaction) was weighted in a 2-ml vial equipped with a magnetic stir bar. Then, the solvent (0.2 ml), aryl halide (0.1 mmol), coupling partner (alkene, boronic acid or alkyne, 0.12–0.2 mmol) and KOAc (11–19 mg, 0.12–0.2 mmol) were added, and the resulting mixture was placed in a pre–heated stainless block reactor at 135 ºC under magnetic stirring. After the desired time, the samples were diluted with dichloromethane (1 ml) and the mixture was stirred, filtered and analyzed by GC and GC–MS after adding *n*–dodecane (22 µl, 0.1 mmol) as an external standard. For kinetics, the reaction was upscaled 10 times and 25 µl aliquots were periodically collected, treated as indicated above, and analyzed by GC.

Reaction order for Pd and Pt clusters. The metal clusters were either leached out from M@EVOH or prepared in situ by endogenous reduction under reaction conditions. In a general experiment, potassium acetate (0.15–0.60 mmol) was added to a glass 2 ml GC vial equipped with a magnetic stirrer. Then, NMP (1 ml), bromo or iodobenzene (0.25–0.75 mmol), *n*–butyl acrylate (0.25–0.75 mmol) and *n*–dodecane as an internal standard were added, after which the vial was closed and stirred at 135 ºC for 10 minutes. Then, either M@EVOH or a 0.1 M solution of $Pd(OAc)_2$ or $Pt(acac)_2$ in NMP (0.0025–0.0075 mmol metal) were added, and aliquots were taken during the first hours of the reaction to measure initial rates.

Computational details. All calculations in this work are based on density functional theory (DFT). Geometry optimizations were carried out employing the Vienna Ab-initio Simulation Package (VASP),[26] spin–polarized and using the PW91 function. The valence density was expanded in a plane wave basis set with a kinetic energy cutoff of 500 eV, and the effect of the core electrons in the valence density was taken into account by means of the projected augmented wave (PAW) formalism. The cluster and molecules were placed in a 20x20x20 $Å^3$ cubic box that was large enough to avoid spurious interactions between periodically repeated systems, and an integration in the reciprocal space was carried out at the Γ k–point of the Brillouin zone. The positions of all atoms in the system were fully optimized without any restriction and all stationary points were characterized by partial Hessian frequency calculations in which the atoms of the cluster remained fixed. The latter were additionally used to calculate the corresponding free energies through partition functions. Transition states were located using the DIMER or CI-NEB algorithms.[27] The Gaussian 09 program package[28] was employed to obtain the molecular orbital distribution of the clusters using the natural bond order (NBO) approach,[29] reoptimizing the structures at the B3LYP[30,31]/LANL2DZ[32,33] level. The ChemCraft[34] program was employed to obtain a graphical representation of the molecular orbitals; in addition, the jmol[35] and MOLDEN[36] programs were used to build and visualize the systems and their frequencies throughout the work.

Microscopy measurements. Electron microscopy studies were performed on an FEI Titan Themis 60–300 Double Aberration Corrected microscope operated at 200kV. The aberrations of the condenser lenses were corrected up to the fourth–order using the Zemlin tableau to obtain a sub–Angstrom electron probe. A condenser aperture of 50 µm yielding an electron probe with a convergence angle of 20 mrad was used. To avoid sample modification under the electron probe, a beam current of 0.025 nA was used. The XEDS hypermaps were recorded using a Super–X EDS detector and 4 window–less XEDS detectors surrounding the TEM sample. The background correction and the deconvolution to extract the contribution of the K lines of S and Ca, respectively, and the L lines of Pt, were carried out using Bruker proprietary software, Esprit 1.94. STEM samples were prepared by depositing small amounts of Pt@EVOH dispersed in organic solution onto holey–carbon-coated Cu grids and leaving the solvent to evaporate. After preparation, samples were maintained in vacuum conditions.

ASSOCIATED CONTENT

Supporting Information Available. The following files are available free of charge. General experimental information, and additional Figures and Tables (PDF).

AUTHOR INFORMATION

Corresponding Author

* To whom correspondence should be addressed. E–mails: boronat@itq.upv.es, anleyva@itq.upv.es, acorma@itq.upv.es.
Phone: +34963877800; Fax: +34963877809.

Notes

The authors declare no competing financial interests.

ACKNOWLEDGMENT

This work was supported by the MINECO (Spain) (Projects CTQ 2017–86735–P and Excellence Unit "Severo Ochoa" SEV–2016–0683). E. F. V. and M. M. thank MINECO for their fellowship SVP–2013–068146 and a predoctoral contract. We thank José M. Coll–Marqués for performing the microfluorescence measurements. Red Española de Supercomputación (RES) and Centre de Càlcul de la Universitat de València are gratefully acknowledged for computational resources.

REFERENCES

(1) Wu, X.–F.; Anbarasan, P.; Neumann, H.; Beller, M. *Angew. Chem. Int. Ed.* **2010**, *49*, 9047–9050.

(2) a) Henderickx, H. J. W.; de Vries, J. G. *Org. Lett.* **2003**, *5*, 3285–3288; b) Leyva–Pérez, A.; Oliver–Meseguer, J.; Rubio–Marqués, P.; Corma, A. *Angew. Chem. Int. Ed*. **2013**, *52*, 11554 –11559.

(3) For references on catalytic Pt clusters see a) Vajda, S.; Pellin, M. J.; Greeley, J. P.; Marshall, C. L.; Curtiss, L. A; Ballentine, G. A.; Elam, J. W.; Catillon–Mucherie, S.; Redfern, P. C.; Mehmood, F.; Zapol, P. *Nat Mater.* **2009**, *8*, 213–216; b) Kimihisa, Y.; Takane, I.; Wang–Jae, C.; Osamu, E.; Hideaki, K.; Masahiro, T.; Atsunori, S. *Nat Chem.* **2009**, *1*, 397–402; c) Yang, C.–T.; Wood, B. C.; Bhethanabotla, V. R.; Joseph, B. *PhysChemChemPhys* **2015**, *17*, 25379–25392; d) Liu, L.; Diaz, U.; Arenal, R.; Agostini, G.; Concepcion, P.; Corma, A. *Nat Mater.* **2017**, *16*, 132–138; e) Rivero–Crespo, M. A.; Leyva–Pérez, A.; Corma, A. *Chem. Eur. J.* **2017**, *23*, 1702–1708; f) Mon, M.; Rivero–Crespo, M. A.; Ferrando–Soria, J.; Vidal–Moya, A.; Boronat, M.; Leyva–Pérez, A.; Corma, A.; Hernandez–Garrido, J. C.; Ló-

pez–Haro, M.; Calvino, J. J.; Ragazzon, G.; Credi, A.; Armentano, D.; Pardo, E. *Angew. Chemie Int. Ed.* **2018**, doi: 10.1002/anie.201801957.
(4) Beletskaya, I. P.; Cheprakov, A. V. *Chem. Rev.* **2000,** *100,* 3009–3066.
(5) Mariampillai, B.; Herse, C.; Lautens, M. *Org. Lett.* **2005**, *7*, 4745–4747.
(6) Oliver–Messeguer, J.; Liu, L.; García–García, S.; Canós–Giménez, C.; Domínguez, I.; Gavara, R.; Doménech–Carbó, A.; Concepción, P.; Leyva–Pérez, A.; Corma, A. *J. Am. Chem. Soc.* **2015**, *137*, 3894−3900.
(7) a) Kelkar, A. A. *Tetrahedron Lett.* **1996**, *37*, 8911–8920; b) Bhanage, B. M; Zhao, F.–G.; Shirai, M.; Arai, M. *Tetrahedron Lett.* **1998**, 39, 9509–9512; c) Kantam, M. L.; Roy, M.; Roy, S.; Subhas, M. S.; Sreedhar, B.; Choudary, B. M. *Synlett* **2006**, *14*, 2266–2268.
(8) a) Wu, Y.; Cai, S.; Wang, D.; He, W.; Li, Y. *J. Am. Chem. Soc.* **2012**, *134*, 8975–8981; b) Shen, Z.; Matsuki, Y.; Shimod, T. *Chem. Commun.* **2010**, *46*, 8606–8608.
(9) a) Corma, A.; Juárez, R.; Boronat, M.; Sánchez, F.; Iglesias, M.; García, H. *Chem. Commun.* **2011**, *47*, 1446–1448, b) Collins, G.; Schmidt, M.; Dwyer, C. O.; Holmes, J. D.; McGlacken, G. P. *Angew. Chem. Int. Ed.* **2014**, *53*, 4142–4145; c) Mozaffari, S.; Li, W.; Thompson, C.; Ivanov, S.; Seifert, S.; Lee, B.; Kovarike, L.; Karim, A. M. *Nanoscale*, **2017**, *9*, 13772–13785.
(10) For Pt see a) Carpenter, M. K.; Moylan, T. E.; Kukreja, R. S.; Atwan, M. H.; Tessema, M. M. *J. Am. Chem. Soc.* **2012**, *134*, 8535−8542; b) Bezbozhnaya, T. V.; Litvinenko, S. L.; Skripnik, S. Y.; Zamashchikov, V. V. Theor. Experim. Chem. **1998**, *34*, 223–226; c) Bezbozhnaya, T. V.; Litvinenko, S. L.; Skripnik, S. Y.; Zamashchikov, V. V., *Russ. J. Gen. Chem.* **1999,** *69*, 1198–1203. For Pd see d) Hyotanishi, M.; Isomura, Y.; Yamamoto, H.; Kawasaki, H.; Obora, Y. *Chem. Commun.* **2011**, *47*, 5750–5752 and ref. 4. For other metals see e) Kawasaki, H. *Nanotechnol Rev*. **2013**, *2*, 5–25 and refs. 5 and 6.
(11) a) Reetz, M. T.; de Vries, J. G. *Chem. Commun.* **2004**, 1559–1563; b) De Vries, J. G. *Dalton Trans.* **2006**, *3*, 421–429; c) Ananikov, V. P.; Beletskaya, I. P. *Organometallics* **2012**, *31*, 1595–1604; d) Mannathan, S.; Raoufmoghaddam, S.; Reek, J. N. H.; de Vries, J. G.; Minnaard, A. J. *ChemCatChem* **2015**, *7*, 3923–3927; e) Huebner, S.; de Vries, J. G.; Farina, V. *Adv. Synth. Catal.* **2016**, *358*, 3–25; f) Astakhov, A. V.; Khazipov, O. V.; Chernenko, A. Y.; Pasyukov, D. V.; Kashin, A. S.; Gordeev, E. G.; Khrustalev, V. N.; Chernyshev, V. M.; Ananikov, V. P. *Organometallics* **2017**, *36*, 1981–1992.
(12) a) Oliver–Meseguer, J.; Dominguez, I.; Gavara, R.; Doménech–Carbó, A.; González–Calbet, J. M.; Leyva–Pérez, A.; Corma, A. *Chem. Commun.* **2017**, *53*, 1116–1119; b) Oliver–Meseguer, J.; Dominguez, I.; Gavara, R.; Leyva–Pérez, A.; Corma, A. *ChemCatChem* **2017**, *9*, 1429–1435.
(13) a) Oliver–Meseguer, J.; Cabrero–Antonino, J. R; Dominguez, I.; Leyva–Pérez, A.; Corma, A. *Science* **2012**, *338*, 1452-1455; b) Bakar, M. A.; Sugiuchi, M.; Iwasaki, M.; Shichibu, Y.; Konishi. K. *Nat. Commun.* **2017**, *8*, 576.
(14) Campos, J.; Ortega–Moreno, L.; Conejero, S.; Peloso, R.; López–Serrano, J.; Maya, C.; Carmona, E. *Chem. Eur. J.* **2015**, *21*, 8883–8896,
(15) Tagge, C. D.; Simpson, R. D.; Bergman, R. G.; Hostetler, M. J.; Girolami, G. S.; Nuzzo, R. G. *J. Am. Chem. Soc.* **1996**, *118*, 2634–2643.
(16) a) Kayahara, E.; Iwamoto, T.; Takaya, H.; Suzuki, T.; Fujitsuka, M.; Majima, T.; Yasuda, N.; Matsuyama, N.; Seki, S.; Yamago, S. *Nat Commun.* **2013**, *4*:2694; b) Liberman–Martin, A. L.; Bergman, R. G.; Tilley, T. D. *J. Am. Chem. Soc.* **2013**, *135*, 9612–9615.
(17) a) Joost, M.; Zeineddine, A.; Estévez, L.; Mallet−Ladeira, S.; Miqueu, K.; Amgoune, A.; Bourissou, D. *J. Am. Chem. Soc.* **2014**, *136*, 14654–14657; b) González–Arellano, C.; Abad, A.; Corma, A.; Garcia, H.; Iglesias, M.; Sanchez, F. *Angew. Chem. Int. Ed.* **2007**, *46*, 1536–1538; c) Boronat, M.; Cómbita, D.; Concepción, P.; Corma, A.; García, H.; Juárez, R.; Laursen, S.; López–Castro, J. D. *J. Phys. Chem. C* **2012**, *116*, 24855–24867.
(18) a) Young, G. B.; Whitesides, G. M. *J. Am. Chem. Soc.* **1978**, *100*, 5808–5815; b) Low, J. J.; Goddard III, W. A. *J. Am. Chem. Soc.* **1986**, *108,* 6115–6128; c) Mueller, C.; Iverson, C. N.; Lachicotte, R. J.; Jones, W. D. *J. Am. Chem. Soc.* **2001**, *123,* 9718–9719.
(19) a) Braunstein, P.; Knorr, M.; Stahrfeldt, T.; *J. Chem. Soc., Chem. Commun.* **1994**, 1913–1914; b) Li, S. F.; Zhao, X. J.; Xu, X. S.; Gao, Y. F.; Zhang, Z. *Phys. Rev. Lett.* **2013**, *111*, 115501–1–5.
(20) Hill, R. H.; Puddephatt, R. J. *J. Am. Chem. Soc.* **1983**, *105*, 5797–5804; b) Morris, R. H. *Chem. Rev.* **2016**, *116*, 8588−8654.
(21) Frasco, D. A.; Mukherjee, S.; Sommer, R. D.; Perry, C. M.; Lambic, N. S.; Abboud, K. A.; Jakubikova, E.; Ison, E. A. *Organometallics* **2016**, *35*, 2435–2445.
(22) Boronat, M.; Lopez-Ausens, T.; Corma, A. *J. Phys. Chem. C* **2014**, *118*, 9018-9029.
(23) Amatore, C.; Pflüger, F. *Organometallics* **1990**, *9*, 2276–2282.
(24) Strieter, E. R.; Bhayana, B.; Buchwald, S. L. *J. Am. Chem. Soc*. **2009**, *131*, 78–88.
(25) Hills, I. D.; Fu, G. C. *J. Am. Chem. Soc.* **2004**, *126*, 13178–13179.
(26) a) Kresse, G.; Furthmüller, J. Phys. Rev. B **1996**, *54*,11169–11186; b) Kresse, G.; Joubert D. Phys. Rev. B **1999**, *59*, 1758–1775.
(27) Henkelman, G.; Jónsson, H. *J. Chem. Phys.***1999**, 111, 7010–7022.
(28) Heyden, A.; Bell, A. T.; Keil, F. J. *J. Chem. Phys.* **2005**, 123, 224101–224114.
(29) Henkelman, G.; Uberuaga, B. P.; Jónsson, H. *J. Chem. Phys.* **2000**, *113*, 9901-9904.
(30) Gaussian 09, Revision C.01, Frisch, M. J.; Trucks, G. W.; Schlegel, H. B.; Scuseria, G. E.; Robb, M. A.; Cheeseman, J. R.; Scalmani, G.; Barone, V.; Mennucci, B.; Petersson, G. A.; Nakatsuji, H.; Caricato, M.; Li, X.; Hratchian, H. P.; Izmaylov, A. F.; Bloino, J.; Zheng, G.; Sonnenberg, J. L.; Hada, M.; Ehara, M.; Toyota, K.; Fukuda, R.; Hasegawa, J.; Ishida, M.; Nakajima, T.; Honda, Y.; Kitao, O.; Nakai, H.; Vreven, T.; Montgomery, J. A., Jr.; Peralta, J. E.; Ogliaro, F.; Bearpark, M.; Heyd, J. J.; Brothers, E.; Kudin, K. N.; Staroverov, V. N.; Kobayashi, R.; Normand, J.; Raghavachari, K.; Rendell, A.; Burant, J. C.; Iyengar, S. S.; Tomasi, J.; Cossi, M.; Rega, N.; Millam, J. M.; Klene, M.; Knox, J. E.; Cross, J. B.; Bakken, V.; Adamo, C.; Jaramillo, J.; Gomperts, R.; Stratmann, R. E.; Yazyev, O.; Austin, A. J.; Cammi, R.; Pomelli, C.; Ochterski, J. W.; Martin, R. L.; Morokuma, K.; Zakrzewski, V. G.; Voth, G. A.; Salvador, P.; Dannenberg, J. J.; Dapprich, S.; Daniels, A. D.; Farkas, Ö.; Foresman, J. B.; Ortiz, J. V.; Cioslowski, J.; Fox, D. J. Gaussian, Inc., Wallingford CT, **2009.**
(31) Reed, A. E.; Weinstock, R. B.; Weinhold, F. Natural Population Analysis. *J. Chem. Phys*. **1985**, *83*, 735–747.
(32) Becke, A. D. *J. Chem. Phys.* **1993**, *98*, 5648-5652.
(33) Lee, C. T.; Yang, W. T.; Parr, R. G. *Phys. Rev. B* **1988**, *37*, 785-789.
(34) Hay, P. J.; Wadt, W. R. Ab Initio Effective Core Potentials for Molecular Calculations -Potentials for the Transition-Metal Atoms Sc to Hg.*J. Chem. Phys.***1985**, *82***,** 270–283.
(35) Hay, P. J.; Wadt, W. R. Ab Initio Effective Core Potentials for Molecular Calculations - Potentials for K to Au including the Outermost Core Orbitals.*J. Chem. Phys.***1985,** *82***,** 299–310.
(36) Schaftenaar G. and Noordik, J. H. Molden: a Pre- and Post-Processing Program for Molecular and Electronic Structures. *J. Comput.-Aided Mol. Design*. **2000**, *14*, 123-134.

Table of contents graphic